nature portfolio

Peer Review File

A robust near-field body area network based on coaxially-shielded textile metamaterial

REVIEWER COMMENTS

Reviewer #1 (Remarks to the Author):

This manuscript reports a body area network (BAN) using coaxially-shielded textile metamaterial. This work sought to address challenges associated with previous works such as external interference and spectral instability and aims to enhance the stability and reliability of near-field communication (NFC)-based technologies. The improved performance is mainly due to the metamaterial's coaxial design, derived from the micro coaxial cable used, which confines the electric field internally and reduces capacitive interaction with the external environment. The textile metamaterial, patterned onto clothing, forms a customizable network that facilitates communication between NFC-enabled devices and battery-free textile NFC sensing nodes. Proof-of-concept demonstrations are provided to show the network's robustness against mechanical deformation and wet conditions. By conducting experimental and theoretical simulation, the findings are well presented. The results are clear, and the conclusions are robust. However, this manuscript in its current form still needs revisions based on the following concerns before it is acceptable for publication in Nature Communications.

1. Although a swimming scenario is depicted in Fig. 1a, it is not presented within the manuscript. To highlight the advantages over previous works, please provide real-time recording in these scenarios to validate the robustness of this work.

2. In Fig. 1j, the authors presented the stability of the metamaterial after repetitive loadings. What about the performance under pressure or under bending?

3. Related to Q3, the authors claim that the spiral-based metamaterial lacks an effective electric field confining mechanism, and therefore is sensitive and spectrally unstable to extraneous loading. Please also provide the performance of the spiral-based one and make a comparison here.

4. In Fig. 2e-g, the authors demonstrated the spectral stability in various scenarios. Is there any metric or method to quantify these variations? Also, the authors claim that it remains functional after machine washing. Please also specify how many washing cycles used here. If only one cycle was used, please also try more cycles to demonstrate its robustness.

5. The authors claim that “This inherently thin and flexible coaxial cable imposes no constraints on human activities when integrated into the textile BAN.” Given the cable material used in this study and its dimension, the reviewer does not believe that there are no constraints on human activities.

6. In Fig. 4g, please clearly label the figures as the reviewer believes that the left panel is from temperature sensor and the right panel is for strain sensor.

Reviewer #2 (Remarks to the Author):

In this manuscript, the authors propose a metamaterial utilizing coaxially-shielded cable to enhance the robustness of near-field body area networks. While the overall objective and the metamaterial design are not novel, the utilization of coaxially-shielded cable presents an interesting approach. Below are my comments.

1. The author should elucidate the design principles and process for the metamaterials utilizing coaxial cable. This includes explaining why the inner conductor is connected with the outer one, methods to adjust the resonant frequency of the coil, the impact of cable structure, dimensions and material on performance, and so on.

2. The observation from Fig.1f suggests that electric confinement occurs only between the inner conductor and the inner surface of the outer conductor. What happens to the outer surface of the outer conductor?

3. “The selection of the micro coaxial cable (diameter 0.99mm) balances ease of fabrication and flexibility, resulting in a lightweight, unperceivable, and comfortable BAN for the user.” “This simple, straightforward design minimizes undesired interference with the surrounding environment with minimal effort, while eliminating lumped elements and fragile internal structures proposed elsewhere25,49. ” Claims regarding the size (millimeter scale) and material (metal and PFA) of the cable conflicting with ease of fabrication, flexibility, and user comfort need scientific validation. Images of the connection and open slit section could provide further clarity.

4. The statement about remarkable spectral stability and insensitivity against extraneous loadings compared to previous efforts should be supported with a direct comparison. Additionally, the potential effects of metallic accessories or clothing with conductive-thread-based material on the proposed MI structure should be addressed.

5. Quantitative characterization, including details of the washing protocol and bending radius in Fig.2e-f, should be provided to enhance the clarity of the results.

6. In Fig.4d, the comparison appears unfair as the quality factor of the conductive thread antenna is low. The authors should compare antennas with similar quality factors for a more accurate assessment.

7. A demonstration of the sensor network in swimming is crucial to support the claim of high robustness.

Reviewer #3 (Remarks to the Author):

This article presents an innovative approach to enhancing the functionality of body area networks (BANs) through the integration of Near-Field Communication (NFC) technology into textile metamaterials. The design and implementation of textile metamaterial patch units to improve the NFC communication range within a BAN is both intriguing and practical, especially for wearable technology applications. The detailed explanation of the metamaterial's structure and its impact on spectral stability and environmental resilience is commendable. However, the scientific contribution of this work appears limited. While the extension of the NFC communication range is noteworthy, similar concepts were demonstrated on BANs before: Nat Commun 13, 2190 (2022); Nat Commun 11, 444 (2020). Here are some technical comments:

1.The paper presents a design of a coaxially-shielded textile metamaterial for near-field communication in BANs. To strengthen the scientific contribution of this paper, it would be beneficial to include comparative analyses with existing BAN technologies, specifically assessing power consumption, data transmission efficiency, and user ergonomics. Additionally, exploring how this NFC-enabled BAN design could be optimized for different use cases, including medical monitoring and athletic performance, could provide a more comprehensive understanding of its applicability and limitations.

2.The demonstration of spectral stability and reduced sensitivity to external conditions, such as water immersion and mechanical deformation, is impressive. However, the paper could provide more quantitative data on the efficiency of energy transfer within the BAN.

3.The work emphasizes the scalability and user-customizability of the metamaterial BAN. It would be valuable to discuss the limitations regarding the maximum number of sensor nodes that can be supported and how the network's performance scales with the number of nodes and the distance covered.

4. The integration of NFC-enabled sensing nodes with commercial NFC readers and smartphones is a practical aspect of this study. However, more details on the compatibility, required modifications, or limitations when integrating with various brands or types of smart devices could provide a clearer view of its applicability in real-world scenarios.

5. While the paper touches on the durability of the metamaterial in harsh conditions, long-term wear and maintenance aspects, such as the ease of repairing or replacing parts of the BAN, are not thoroughly discussed. Insights into these practical aspects would enhance the understanding of the technology's viability for everyday use.

To the Reviewers,

We thank all the reviewers for their insightful and constructive comments on out manuscript. Please find below a point-by-point response to each reviewer. The original comment from each reviewer is marked in green. The specific changes made to the manuscript are highlighted in blue (Reviewer #1: Page 2-7; Reviewer #2: Page 8-18; Reviewer #3: Page 19-27).

Reviewer #1:

This manuscript reports a body area network (BAN) using coaxially-shielded textile metamaterial. This work sought to address challenges associated with previous works such as external interference and spectral instability and aims to enhance the stability and reliability of near-field communication (NFC)-based technologies. The improved performance is mainly due to the metamaterial's coaxial design, derived from the micro coaxial cable used, which confines the electric field internally and reduces capacitive interaction with the external environment. The textile metamaterial, patterned onto clothing, forms a customizable network that facilitates communication between NFC-enabled devices and battery-free textile NFC sensing nodes. Proof-of-concept demonstrations are provided to show the network's robustness against mechanical deformation and wet conditions. By conducting experimental and theoretical simulation, the findings are well presented. The results are clear, and the conclusions are robust. However, this manuscript in its current form still needs revisions based on the following concerns before it is acceptable for publication in Nature Communications.

We thank the reviewer for affirming the potential interest of the concept presented in out manuscript. As detailed below, we have carefully made adjustments to the manuscript and supplemented additional results addressing the specific comments provided.

1. Although a swimming scenario is depicted in Fig. 1a, it is not presented within the manuscript. To highlight the advantages over previous works, please provide real-time recording in these scenarios to validate the robustness of this work.

We thank the reviewer for suggesting demonstrations in swimming scenarios. In response, we conducted additional experiment as presented in Supplementary Figure 18. A metamaterial BAN was constructed on the back of the athletic pants. The reading device (smartphone) was sealed in a waterproof pouch and placed on the left calf to wirelessly power the sensing node on the right knee. Several battery-free energy-harvesting LED nodes were placed along the BAN, indicating robust underwater power transfer. The entire system, including the reader, nodes and the metamaterial, was immersed in water. Bending was then performed at the right knee to simulate a swimming scenario, with the resistance values of the strain sensor indicating the degree of knee flexion. The results demonstrate that the metamaterial remains robust and reliable in an underwater environment. We have added a statement to address these results:

"Additionally, to further demonstrate the robustness of the BAN, we construct a metamaterial-enabled BAN on athletic pants for real-time data readout underwater, simulating a swimming scenario. The metamaterial remains functional due to its improved spectral stability, enabling uninterrupted real-time data readout using a smartphone while powering several LED energy-harvesting nodes (Supplementary Fig. 18)." **(Page 21)**

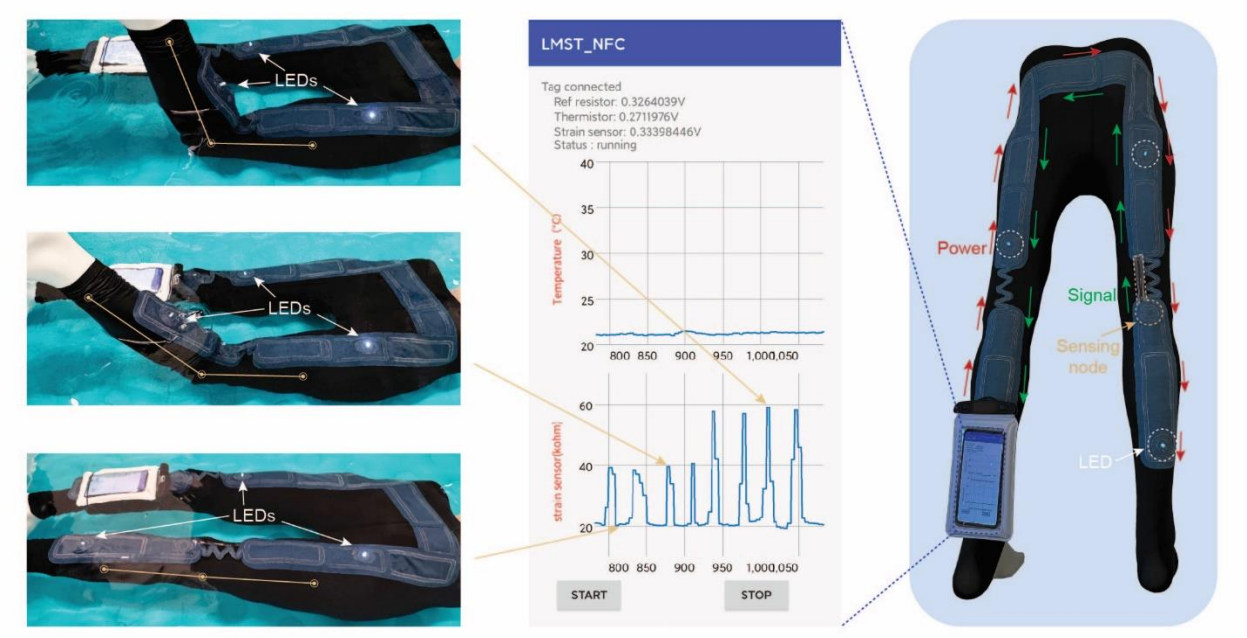

Supplementary Figure 18. Real-time data readout performed underwater. Benefiting from the introduced spectral stability, the metamaterial-enabled BAN promotes reliable underwater real-time data readout. The smartphone, placed in a waterproof pouch, continuously retrieve data from the sensing node, with the strain sensor's resistance indicating the degree of knee flexion, while powering several distant battery-free energy-harvesting LED nodes placed along the BAN.

2. In Fig. 1j, the authors presented the stability of the metamaterial after repetitive loadings. What about the performance under pressure or under bending?

We thank the reviewers for this suggestion. We conducted addition measurements as presented in Supplementary Figure 13. We first measured the resonance frequency of a single metamaterial unit cell flexed into an arc shape with increasing central angle, the metamaterial only exhibits a 1.33% (0.18 MHz) frequency shift when the angle reaches to 240°, demonstrating its resilience against frequency detuning when conformed to anatomic regions with large curvatures (Supplementary Fig. 13a). More pronounced frequency shifts occurred when the unit cell was folded at its center due to increased magnetic flux overlap (destructive interference), disrupting its self-inductance (Supplementary Fig. 13b). Specifically, folding by 165° leads to a 10.41% (1.412 MHz) shift, and when half-folded, the resonance peak almost entirely disappears due to a complete cancelation of the magnetic flux. This indicates that when placing the metamaterial on joints, where wide and random flexion frequently happens, the metamaterial may experience huge frequency deviations or even cease to resonate, highlighting the importance of adopting the stretchable join unit.

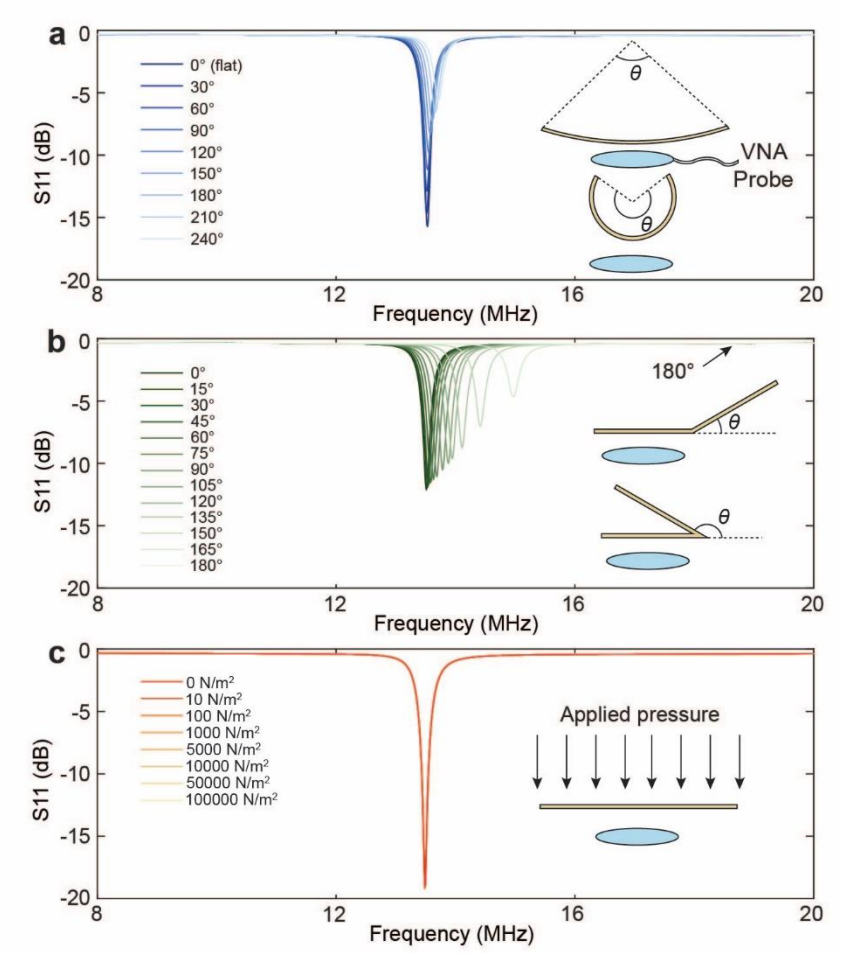

Supplementary Figure 13. Frequency response of the metamaterial unit cell under deformation and pressure. a The unit cell remains spectral stable when flexed to an arc shape, exhibiting only a 1.33% (0.18 MHz) resonance frequency shift when the central angle increase to 240°. **b** Significant frequency shifts occur when the unit cell is folded, due to substantial cancellation of magnetic flux through the resonator loop, emphasizing the need for stretchable joint units at joint positions. **c** The resonance frequency stays stable under pressures up to 100,000 N/m², indicating that such pressure does not cause noticeable deformation or damage to the coaxial cable's internal structure.

In Fig. 1j, we demonstrate the mechanical stability of a metamaterial unit cell after repetitive bending and repetitive vertical loading. We would like to emphasize that although we characterize the repetitive vertical loading by the calculated vertical pressure, the condition of the metamaterial unit cell is essentially being bent, as the unit cell is half-folded. This characterization actually represents a more extreme bending scenario, further stressed by direct external pressure applied. The durability of the metamaterial is enhanced by the stranded configuration of metal thread conductors in the cable, shielded and protected by PFA insulation and jacket, making them highly resistant to fractures and deformations. Additionally, we measured the resonance frequency of an unfolded metamaterial unit cell under pressure up to100000 N/m^2, roughly equivalent to the weight of an 80 kg human being uniformly distributed over one unit cell (Supplementary Fig. 13c). The resonance frequency remains stable, indicating that pressure at this level does not cause noticeable deformation or damage to the coaxial cable's internal structure. Additional details on resilience against deformation and pressure have been included in the manuscript:

"The metamaterial, when integrated into textile layers, exhibits outstanding flexibility and can be seamlessly integrated onto pre-existing clothing, withstanding moderate mechanical deformation and pressure resulting from natural human motion (Supplementary Figure 13a, c)." **(Page 13)**

"The shoulder joint experiences wide and random flexion during human motion and exercise, leading to potential concerns about the deviation of the metamaterial's resonance frequency, especially with random overlap or creasing of clothing at such joints (Supplementary Fig. 13b). This could potentially interrupt continuous signal monitoring." **(Page 13)**

3. Related to Q3, the authors claim that the spiral-based metamaterial lacks an effective electric field confining mechanism, and therefore is sensitive and spectrally unstable to extraneous loading. Please also provide the performance of the spiral-based one and make a comparison here.

We thank the reviewer for suggesting comparison with the metamaterial's counterparts to support our claim.

We conducted additional experiments, as shown in Supplementary Figure 1. A spiral-based resonator was constructed by milling cladded copper on a 1.5mm-thick FR-4 substrate, optimized to match the dimension of the coaxially-shielded design while resonating at 13.56 MHz. Frequency response of these two resonator configurations is measured under four loading conditions: affixed to acrylic board ($\varepsilon \approx 3$), affixed to 1% agarose gel ($\varepsilon \approx 80$), immersed in deionized (DI) water, and immersed in 0.9% saline. The coaxially-shielded resonator exhibits minimal frequency shifts of 0, 0.15, 3.72, and 4.96%, respectively (Supplementary Fig. 1a). In contrast, the spiral resonator shows larger shifts of 8.67% and 35.76% on acrylic and agarose, respectively, and failed to maintain a detectable resonance in DI water and saline (Supplementary Fig. 1b).

Additional tests on the spiral-based resonator were conducted after applying two-sided sealing with a 1.5mm-thick acrylic tape, intended to create a less harsh loading condition by enclosing it with low-permittivity material and preventing potential short-circuits. Nevertheless, the resonator still exhibits frequency shifts of 3.06, 18.89, 42.84 and 47.15% under the same conditions (Supplementary Fig. 1c). The observed difference between the coaxially-shielded resonator and its spiral-based counterpart demonstrates effectiveness of the introduced electric field confining mechanism. We have addressed these results when comparing the two resonators:

"Additionally, this electric field confinement effect does not adversely impact the metamaterial's predominant magnetic resonance, resulting in a comparable inductive magnetic field to conventional copper spiral-based metamaterial (Fig. 1g, i). The latter lacks an effective electric field confining mechanism, rendering it substantially more sensitive and spectrally unstable to extraneous loading (Supplementary Fig. 1)." **(Page 8)**

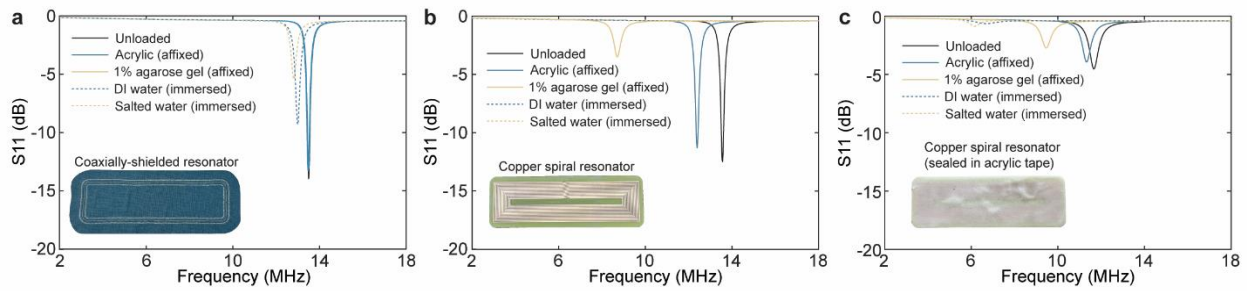

Supplementary Figure. 1 Comparison of frequency response between coaxially-shielded resonator and conventional spiral-based resonator. a The coaxially-shielded resonator exhibits frequency shifts of 0, 0.15, 3.72 and 4.96% when affixed to acrylic, affixed to 1 % agarose gel, immersed in deionized (DI) water, and immersed in 0.8% salted water. **b** The conventional copper spiral resonator (milled on 1.5mm-thick FR-4, optimized to the same dimension and frequency as the coaxially-shielded resonator) exhibits frequency shifts of 8.67 and 35.76% when affixed to acrylic and agarose gel, respectively, and fails to maintain detectable resonance when immersed in DI water or saline. **c** After applying two-sided sealing with a 1.5 mm-thick acrylic tape, the copper spiral resonator still exhibits frequency shifts of 3.06, 18.89, 42.84 and 47.15% under these loadings.

4. In Fig. 2e-g, the authors demonstrated the spectral stability in various scenarios. Is there any metric or method to quantify these variations? Also, the authors claim that it remains functional after machine washing. Please also specify how many washing cycles used here. If only one cycle was used, please also try more cycles to demonstrate its robustness.

We thank the reviewer for addressing importance of metrics for the presented variations and washing tests. We have supplemented a statement in the Methods Section and Supplementary Figure 25 for clarifications:

"For measurement conducted in Fig. 2e-g, the metamaterial was flexed into the desired shape and conformed to plastic scaffolds (Supplementary Fig. 25)." **(Page 26)**

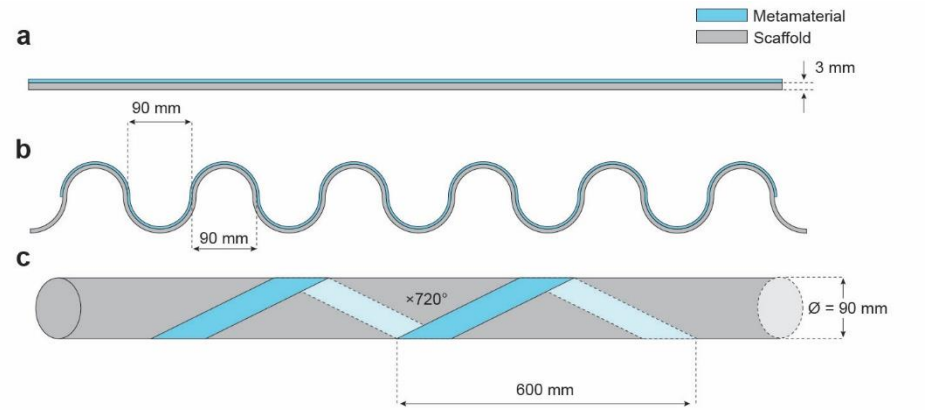

Supplementary Figure 25. **Experimental setup adopted in Figure 2e-g. a** In Fig. 2e, the metamaterial was placed on an acrylic board. **b** In Fig. 2f, the metamaterial was placed on a 3D-printed serpentine PLA scaffold. **c** In Fig. 2g, the metamaterial was wound around an acrylic pipe.

We have updated the Methods Section with information on our washing test protocols:

"For the washing tests, five cycles were conducted in accordance with the ISO 6330 standard for domestic washing and drying procedures for textile testing. The metamaterials were combined with other clothing in a household washing machine (Whirlpool) to form a load of 2 kg. Each washing cycle was set to 34 minutes at 40°C, with 20 g of liquid detergent added (Tide, Procter & Gamble). After each cycle, the metamaterial was air dried." **(Page 26)**

It's important to note that the conductors in the metamaterials are well-protected by a waterproof PFA jacket and heat shrink tubing, both chemically inert to detergent components. Additionally, the adopted textile substrate with the embroidered duct also adds to the overall mechanical strength of the resonator structure.

5. The authors claim that "This inherently thin and flexible coaxial cable imposes no constraints on human activities when integrated into the textile BAN." Given the cable material used in this study and its dimension, the reviewer does not believe that there are no constraints on human activities.

We thank the reviewer for raising concerns about potential constraints posed by the metamaterial. We acknowledge that our initial statement may have been overly definitive. Our choice of the dimension of commercial coaxial cable was a compromise between ease of fabrication and cable flexibility. We would like to clarify that our technique for constructing coaxially-shielded resonators, metamaterials, and antennas is adaptable to various cable dimensions and conductor materials. The proposed structure is topologically robust, regardless of the type of cable used. Industries offer micro coaxial cable solutions with diameter as small as 160 µm, offering versatile design choices at the expense of added manufacturing complexity. For example, we have demonstrated that direct embroidery with thinner coaxial cables, such as those with a 360 µm diameter, is feasible (Supplementary Fig. 21); however, these thinner cables require careful handling during stripping and trimming to prevent damage to the stranded conductor threads. We have changed the previous description to "*This inherently thin and flexible coaxial cable imposes minimal constraints on human activities when integrated into the textile BAN*" We have carefully reviewed the manuscript to ensure that it is free of any similarly conclusive statements.

6. In Fig. 4g, please clearly label the figures as the reviewer believes that the left panel is from temperature sensor and the right panel is for strain sensor.

We thank the reviewer for pointing out this oversight, the right panels are now labeled with the resistance values of the strain sensors.

Reviewer #2:

In this manuscript, the authors propose a metamaterial utilizing coaxially-shielded cable to enhance the robustness of near-field body area networks. While the overall objective and the metamaterial design are not novel, the utilization of coaxially-shielded cable presents an interesting approach. Below are my comments.

1. The author should elucidate the design principles and process for the metamaterials utilizing coaxial cable. This includes explaining why the inner conductor is connected with the outer one, methods to adjust the resonant frequency of the coil, the impact of cable structure, dimensions and material on performance, and so on.

We thank the reviewer for addressing the importance of clearly articulating the design principles and processes for the metamaterial. In response, we have included Supplementary Note 1, Supplementary Figures 3, 4, 5 to further detail the design logic and optimization process.

In our design, the near-field metamaterial is composed of resonating loops that form collective resonating modes. The interaction among adjacent unit cells is primarily inductive, dominated by the oscillating magnetic field within each unit cell. The oscillating magnetic field is invariably accompanied by a varying electric field, as dictated by the electromagnetic theorem. Consequently, the magneto-inductive wave in the metamaterial also induces a redistribution and amplification of the electric field in the vicinity of the metamaterial. The amplified electric field can interact with the dielectric and conductive properties of the surrounding media, contributing to the spectral instability and dielectric/conductive loss.

Electric fields are inherently bound by capacitors, with their capacitance indicating the ability to store electric charge. Hence, a significant self-capacitance in a magnetic metamaterial, which is well-protected and less exposed, is advantageous for achieving desired spectral stability.

Coaxial cables, known for their signal preservation over long distances, are traditionally employed for RF applications, effectively block electromagnetic interference due to their conductive outer layers (shielding layers). Simultaneously, the potential difference between the inner and outer conductors in coaxial cables creates a significant electric field, introducing substantial shunt capacitance. This capacitance is vital for signal integrity and forms the basis for integrating it into the metamaterial's self-capacitance to enhance the robustness of near-field BAN designs.

We observed that directly applying coaxial cable as a conductor to construct conventional helical/spiral resonators does not yield the desired effect (Supplementary Fig. 3), primarily because the well-isolated inner conductor is not sufficiently perceived or excited by the external excitation. Under this configuration, the resonator essentially behaves like a helical resonator with a thicker wire, the current on the outer surface of the outer conductor follows the sinusoidal pattern conventionally found on a helical resonator. By welding the inner and outer conductors together, the inner conductor is thereby electrically exposed, enabling it to participate in resonance, facilitating the desired electric field confinement effect. We have also included an equivalent circuit model to aid understanding of the coaxially-shielded metamaterial and its coupling mechanism (Supplementary Fig. 4).

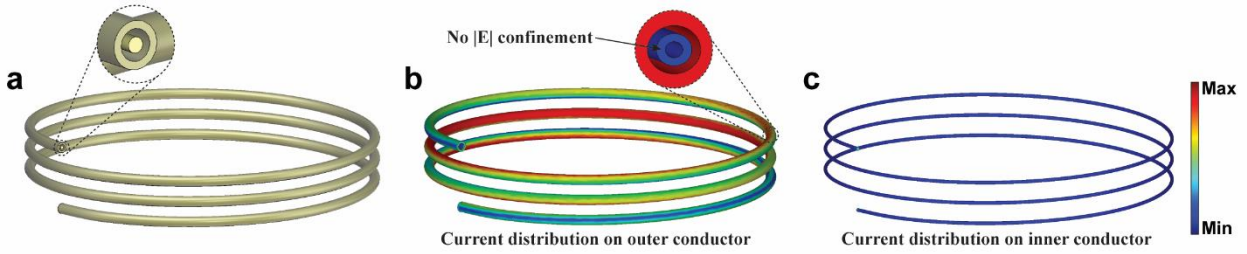

Supplementary Figure 3. **Using coaxial cable to construct helical resonator without welding junction.** **a** Helical resonator model adopted for simulation. **b** The oscillating current is exclusively distributed on the outer surface of the outer conductor. No desired electric field confinement is observed. **c** No current is observed on the inner conductor due to the shielding effect of the outer conductor.

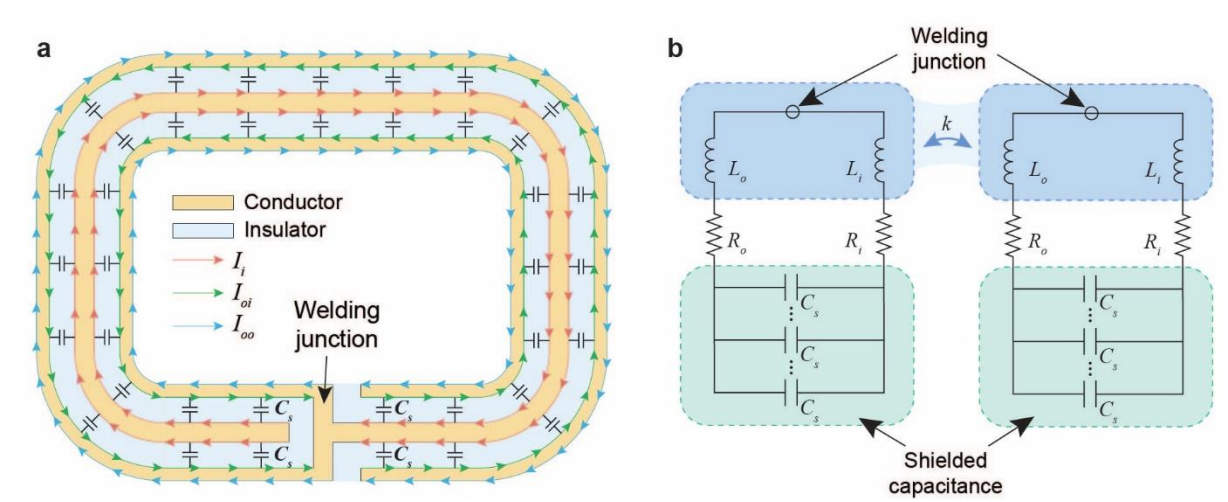

Supplementary Figure 4. **Equivalent circuit model of the coaxially-shielded metamaterial.** **a** Current distribution in the cross-sectional view of the metamaterial unit cell, C_s denotes the structural self-capacitance between the conductor layers. **b** Equivalent circuit diagram reveals the coupling mechanism of the coaxially-shielded metamaterial. L_i and R_i denote the inductance and resistance of the inner conductor, while L_o and R_o represent those of the outer conductor. k denotes the inter-unit cell coupling. C_s represent the structural self-capacitance that is confined and isolated within the insulating layer.

The resonance frequency and performance can be affected by several inherent parameters of the adopted coaxial cable, including the conductor material, insulator material, inner conductor radius T_i, insulator thickness T_{ins}, and outer conductor thickness T_o (Supplementary Fig. 5a). The conductor's conductivity has a direct impact on the ohmic loss and thereby the performance (Supplementary Fig. 5b). The adopted cable conductor is silver-plated copper, commonly employed in low-loss cable design; it combines silver's high conductivity and resistance to corrosion with copper's lower cost.

The inner and outer conductor are separated by an insulation layer, typically composed of a polymer material with a permittivity value between 2 and 3, constituting a capacitor that provides the electric field confinement. The permittivity of the insulator, inner conductor radius, and insulator thickness all have impact on its capacitance and the performance of the metamaterial (Supplementary Fig. 5c-e). The outer conductor thickness, however, presents negligible effect as it does not significantly alter the layered internal structure (Supplementary Fig. 5f). These parameters are pre-determined by the cable manufacture, and cannot be individually altered to adjust the metamaterial's frequency.

The metamaterial's resonance frequency is optimized through the cable length and the unit cell's covered area. The design aims to maximize magnetic field enhancement capability within its coverage area while accommodating practical considerations. For instance, the shorter edges of the metamaterial should be of comparable dimension to the smallest deployable anatomy like the calf or forearm, and should be wide enough to cover the sensing nodes. Meanwhile, the longer edges of the metamaterial should to be sufficiently long to avoid the excessive usage of more unit cells. The adopted dimension (200 mm × 55 mm) enables frequency match while striking a balance between magnetic field enhancement and practicality for integration onto existing clothing (Supplementary Fig. 5g-i).

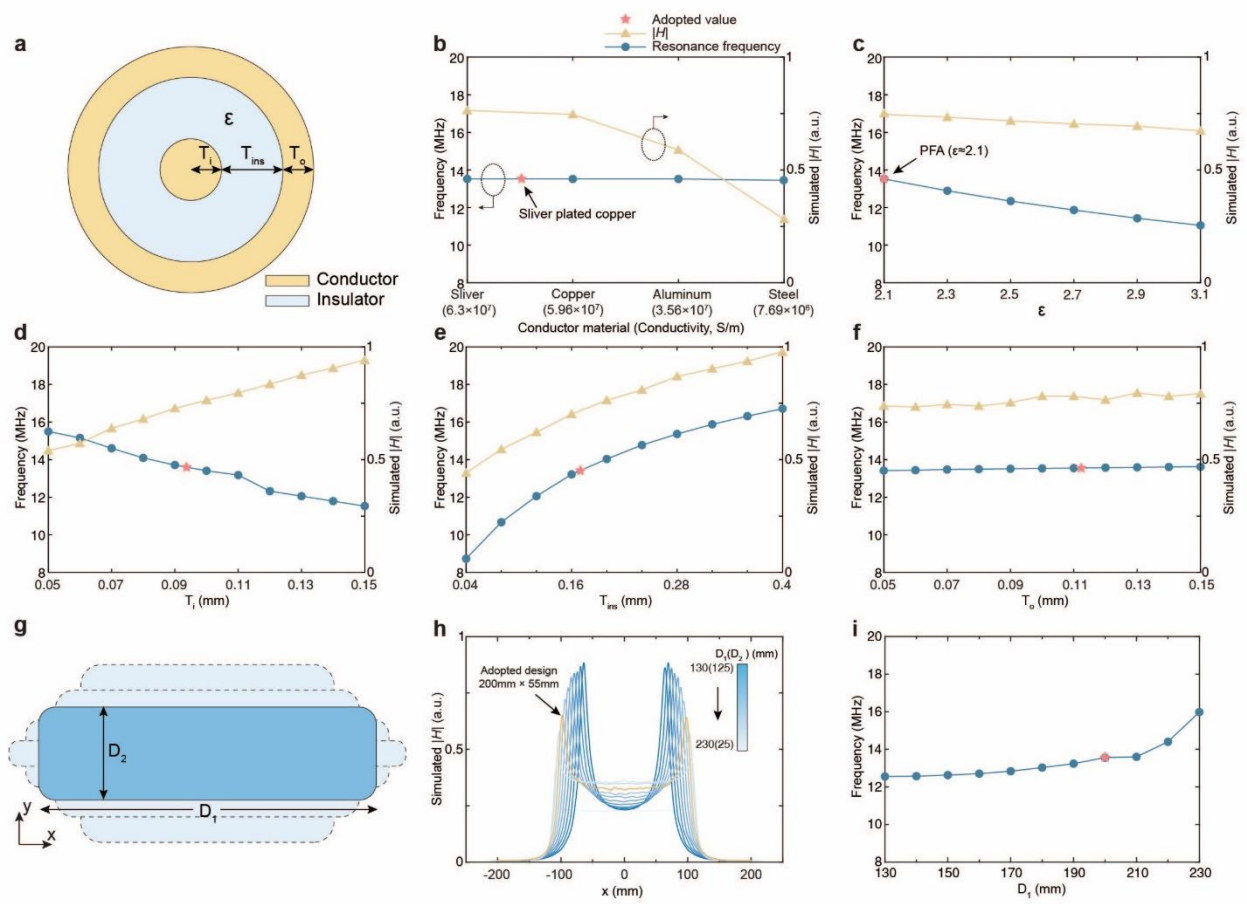

Supplementary Figure 5. **Optimization of the metamaterial design. a** Cross-sectional view of the coaxial cable. **b-f** Impact of the coaxial cable's parameters on the resonance frequency and the magnetic field strength at the center point (x = 0, y = 0) of the metamaterial plane, including conductor material (**b**), insulator material (characterized by ε) (**c**), inner conductor radius T_i (**d**), insulation thickness T_{ins} (**e**), and outer conductor thickness T_o (**f**). **g-i** Impact of the metamaterial's coverage on the magnetic field distribution (**h**) and resonance frequency (**i**) while maintaining the perimeter.

2. The observation from Fig.1f suggests that electric confinement occurs only between the inner conductor and the inner surface of the outer conductor. What happens to the outer surface of the outer conductor?

We have included additional simulation results, which include a zoomed-in view of the simulated electric field in Fig. 1f, with detailed dimension of the cable precisely mapped onto the electric field distribution profile (Supplementary Fig. 7). This result is addressed in the manuscript along with the discussion about Fig. 1f. The electric field confined inside the insulating layer is substantially higher than that in the region surrounding the outer conductor. While a parasitic electric field (≈ 29% of the maximum value within the insulating layer) emerges between adjacent turns of the resonator, this region is predominantly occupied by the cable jacket. Outside this area, the electric field around the outer conductor significantly drops to just 2.3% of the maximum observed within the insulating layer.

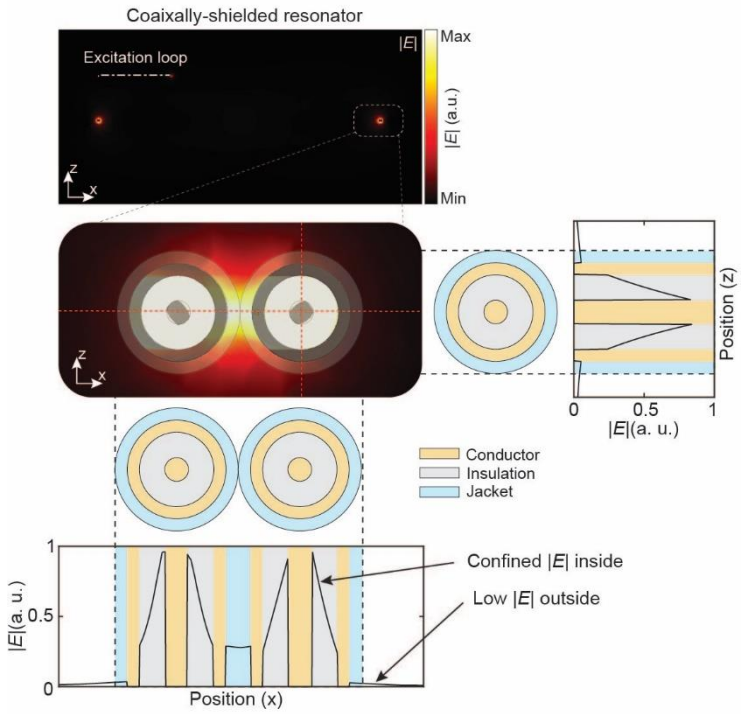

Supplementary Figure 7. **Electric field distribution in proximity to the coaxial cable.** The electric field across the cable's cross-section (red dashed lines) is plotted and precisely mapped to the cable structure, indicating that the majority of the electric field is confined between the two conductor layers.

3. "The selection of the micro coaxial cable (diameter 0.99mm) balances ease of fabrication and flexibility, resulting in a lightweight, unperceivable, and comfortable BAN for the user." "This simple, straightforward design minimizes undesired interference with the surrounding environment with minimal effort, while eliminating lumped elements and fragile internal structures proposed elsewhere25,49." Claims regarding the size (millimeter scale) and material (metal and PFA) of the cable conflicting with ease of fabrication, flexibility, and user comfort need scientific validation. Images of the connection and open slit section could provide further clarity.

We thank the reviewer for suggesting further clarification of these statements.

Constructing the proposed coaxially-shielded resonator involves stripping, trimming, welding and reinforcing of the cable. We have provided a detailed, step-by-step demonstration of constructing a resonator (Supplementary Fig. 23), offering further clarity on the connection at the open slit.

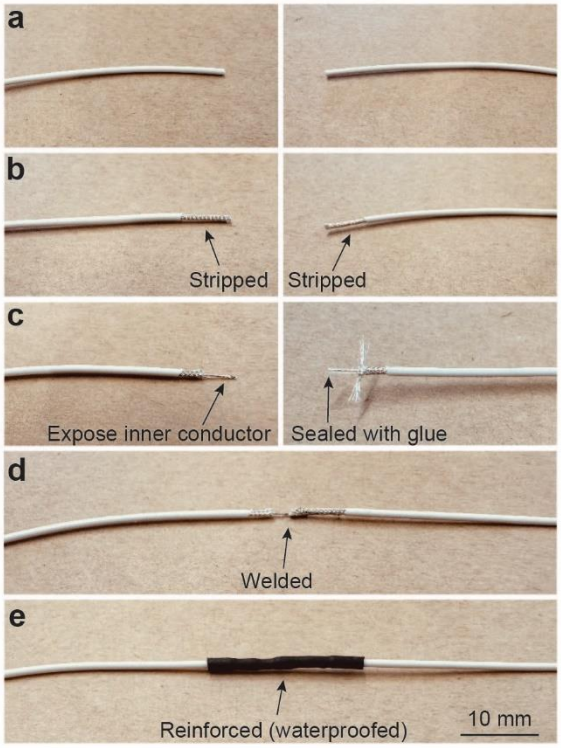

Supplementary Figure 23. Step-by-step demonstration for constructing a coaxially-shielded resonator at the open slit. a Two ends of a cable segment. **b** The jacket is stripped to expose the outer conductor. **c** The outer conductor and insulation are stripped to expose the inner conductor on the left; the end of the inner conductor is sealed with glue to prevent short circuits on the right. **d** The inner conductor on the left is welded to the outer conductor on the right. **e** The open slit is reinforced with a waterproof heat shrink tubing.

Furthermore, the statement regarding the selection of the cable and its impact on ease of fabrication simply indicates that operating on a relatively thicker cable is more convenient. For example, commonly encountered thicker coaxial cable groups, including RG58, RG174, RG178, etc., can typically be stripped and trimmed with a commercial cable stripper. However, for thinner commercial micro coaxial cables, such as the 9434 series from Alpha Wire that we used, manual stripping and trimming with a precision blade is recommended to avoid damaging the stranded thin wires in the shielding layer. We have revised the addressed statement:

"The selected dimension of the micro coaxial cable (diameter 0.99mm) balances ease of fabrication and flexibility, resulting in a lightweight, nearly imperceptible, and comfortable BAN for the user." **(Page 23)**

We have added the following statement in the Method Section for clarification:

"Constructing the coaxially-shielded metamaterial involves stripping, trimming, welding and reinforcement of the cable (Supplementary Fig. 23) While commercial cable strippers suited for the adopted wire gauge are available, using a precision blade for these procedures is recommended to avoid damaging the stranded thin metal wires." **(Page 24)**

Additionally, the material of the cable does not conflict ease of fabrication. Specifically, the conductor material, silver plated copper, is a widely adopted configuration in cable manufacturing industry. The insulation and jacket material, PFA, are comparable in hardness and strength to other typical insulation

materials used in coaxial cables (Table R1). Regarding the trade-off between cable size, flexibility, and user comfort, the authors believe this relationship is straightforward: thinner wire with the same composition is naturally more flexible and less noticeable when worn.

Table R1. **Hardness and Ultimate tensile strength of commonly adopted material for coaxial cable insulation and jacket.** (https://www.matweb.com/index.aspx)

Material	PFA	PTFE	HDPE	FEP	PVC
Hardness (Shore D)	57.6	58.2	64.4	55.8	77.4
Ultimate tensile strength (MPa)	27.1	25.6	28.6	24.3	24.0

4. The statement about remarkable spectral stability and insensitivity against extraneous loadings compared to previous efforts should be supported with a direct comparison. Additionally, the potential effects of metallic accessories or clothing with conductive-thread-based material on the proposed MI structure should be addressed.

We thank the reviewer for suggesting comparison with the metamaterial's counterparts to support our claim. We have added additional comparison in Supplementary Figure 1 as requested.

Conventional inductive patterns for near-field applications typically use spiral-based resonators, which do not achieve the level of spectral stability provided by the coaxially-shielded internal designs. A spiral-based resonator was constructed by milling cladded copper on a 1.5mm-thick FR-4 substrate, optimized to match the dimension of the coaxially-shielded design while resonating at 13.56 MHz. Frequency response of these two resonator configurations is measured under four loading conditions: affixed to acrylic board ($\varepsilon \approx 3$), affixed to 1% agarose gel ($\varepsilon \approx 80$), immersed in deionized (DI) water, and immersed in 0.9% saline. The coaxially-shielded resonator exhibits minimal frequency shifts of 0, 0.15, 3.72, and 4.96%, respectively (Supplementary Fig. 1a). In contrast, the spiral resonator shows larger shifts of 8.67% and 35.76% on acrylic and agarose, respectively, and failed to maintain a detectable resonance in DI water and saline (Supplementary Fig. 1b).

Additional tests on the spiral-based resonator were conducted after applying two-sided sealing with a 1.5mm-thick acrylic tape, intended to create a less harsh loading condition by enclosing it with low-permittivity material and preventing potential short-circuits. Nevertheless, the resonator still exhibits frequency shifts of 3.06, 18.89, 42.84 and 47.15% under the same conditions (Supplementary Fig. 1c). The observed difference in the performance of the coaxially-shielded resonator compared to the spiral-based counterpart prove the effectiveness of the introduced electric field confining mechanism. We have addressed these results it the manuscript:

"In sharp contrast to previous efforts to develop NFC-enabled wearable BANs based on spiral-based inductive patterns[24-26], the metamaterial proposed herein demonstrate remarkable spectral stability and insensitivity against extraneous loadings (Supplementary Fig. 1)." **(Page 4)**

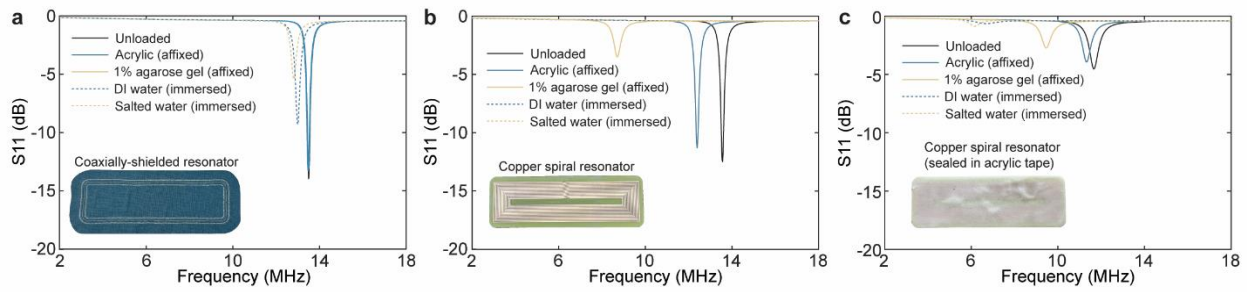

Supplementary Figure. 1 Comparison of frequency response between coaxially-shielded resonator and conventional spiral-based resonator. a The coaxially-shielded resonator exhibits frequency shifts of 0, 0.15, 3.72 and 4.96% when affixed to acrylic, affixed to 1 % agarose gel, immersed in deionized (DI) water, and immersed in 0.8% salted water. **b** The conventional copper spiral resonator (milled on 1.5mm-thick FR-4, optimized to the same dimension and frequency as the coaxially-shielded resonator) exhibits frequency shifts of 8.67 and 35.76% when affixed to acrylic and agarose gel, respectively, and fails to maintain detectable resonance when immersed in DI water or saline. **c** After applying two-sided sealing with a 1.5 mm-thick acrylic tape, the copper spiral resonator still exhibits frequency shifts of 3.06, 18.89, 42.84 and 47.15% under these loadings.

Regarding the potential effects from metallic accessories, additional experiments were conducted and demonstrated in Supplementary Figure 12. The experimental setup includes an inline metamaterial composed of 7 unit cells, covering a distance of 1 m. First, a series of common metallic clothing accessories, including metallic buttons and zippers (zinc alloy) were placed near the metamaterial in three random configurations. The transmission coefficients measured under these scenarios indicate that these accessories induce a minimal and negligible effect on the BAN, with NFC connectivity remaining unaffected when using a reader and tag at each end of the metamaterial (Supplementary Fig. 12a-c).

Next, a conductive non-woven fabric (Series 4770, polyester with Copper/Nickle coating, surface resistivity: $< 0.03\Omega/sq$, thickness: 0.19 mm, Holland Shielding Systems BV) was applied to investigate the effect from conductive-thread-based materials. Covering the entire metamaterial with this fabric disrupted NFC connectivity until the metamaterial was raised by 1.5 cm (Supplementary Fig. 12d-f). This result is expected and consistent with conventional near-field system responses, as large conductive materials act like electromagnetic interference (EMI)/radio-frequency interference (RFI) shields, strongly deviating the resonance frequency of the metamaterial while precluding the propagation of the NFC signal. However, the BAN demonstrated moderate resilience when exposed to smaller pieces or patches of the conductive fabric (Supplementary Fig. 12g-i). We have added discussion on the metallic accessories in the manuscript.

"Additionally, as with conventional near-field systems, the metamaterial is sensitive to the proximity of large pieces of conductive material, such as conductive-thread-based fabric, which essentially behave like RF shields, altering the metamaterial's resonance frequency while precluding NFC signal propagation. However, the metamaterial remains reliable when in contact with smaller metallic accessories (zippers and buttons) or conductive fabric patches (Supplementary Fig. 12)." **(Page 13)**

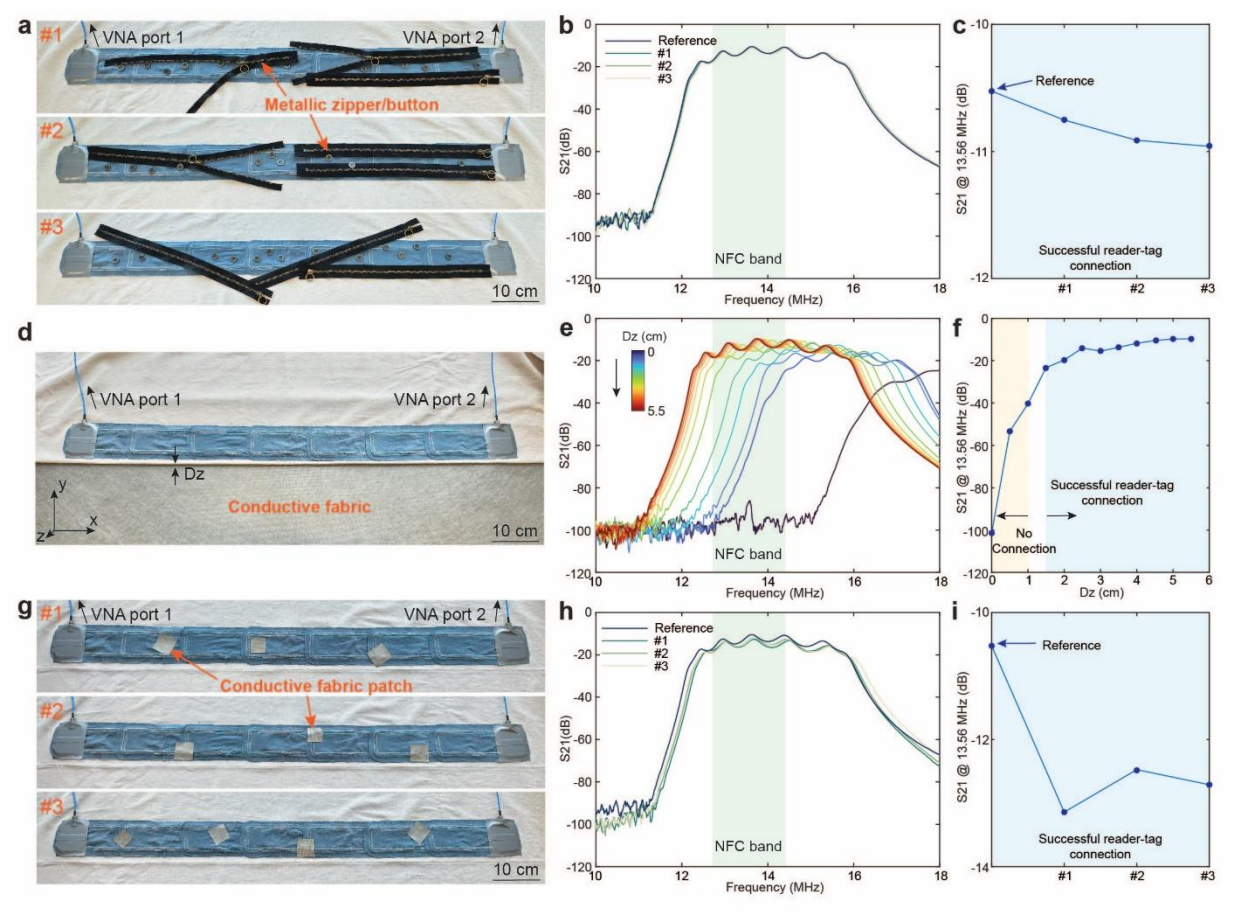

Supplementary Figure 12. Effects of metallic accessories and conductive fabric. a-c The 7-unit inline metamaterial is insensitive to the proximity of metallic zippers and buttons (zinc alloy), maintaining a stable transmission profile under three random configurations, with NFC connection preserved when placing a reader and tag at each end of the metamaterial. **d-f** Contact with a piece of conductive fabric (Series 4770, polyester with Copper/Nickle coating, surface resistivity: $< 0.03\Omega/sq$, thickness: 0.19 mm, Holland Shielding Systems BV) covering the entire metamaterial substantially shifts the resonance frequency, disrupting NFC connection until the metamaterial is raised by 1.5 cm vertically. **g-i** The metamaterial demonstrates resilience against smaller conductive fabric patches, showing less significant resonance frequency shifts, and maintains unhindered NFC connection under three random configurations.

5. Quantitative characterization, including details of the washing protocol and bending radius in Fig.2e-f, should be provided to enhance the clarity of the results.

We have supplemented a statement in the Methods Section and Supplementary Fig. 25 as requested:

"For measurement conducted in Fig. 2e-g, the metamaterial was flexed into the desired shape and conformed to plastic scaffolds (Supplementary Fig. 25)." **(Page 26)**

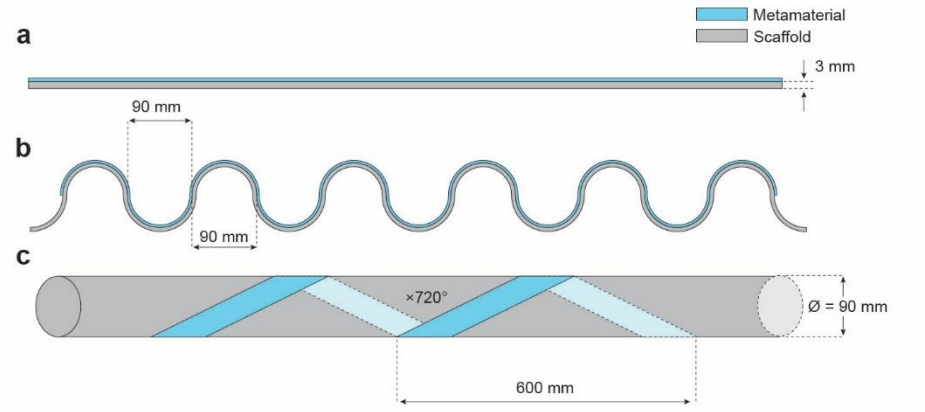

Supplementary Figure 25. **Experimental setup adopted in Figure 2e-g. a** In Fig. 2e, the metamaterial was placed on an acrylic board. **b** In Fig. 2f, the metamaterial was placed on a 3D-printed serpentine PLA scaffold. **c** In Fig. 2g, the metamaterial was wound around an acrylic pipe.

We have also supplemented the washing protocol in the Methods Section:

"For the washing tests, five cycles were conducted in accordance with the ISO 6330 standard for domestic washing and drying procedures for textile testing. The metamaterials were combined with other clothing in a household washing machine (Whirlpool) to form a load of 2 kg. Each washing cycle was set to 34 minutes at 40°C, with 20 g of liquid detergent added (Tide, Procter & Gamble). After each cycle, the metamaterial was air dried." **(Page 26)**

6. In Fig.4d, the comparison appears unfair as the quality factor of the conductive thread antenna is low. The authors should compare antennas with similar quality factors for a more accurate assessment.

We agree with the reviewer's observation that the conductive thread antenna has very low quality factor, primarily due to the higher resistance typically found in commercial conductive threads. Conductive thread is often applied to construct antennas for wearable NFC applications. For reference, Jiang *et al.* reported a silver-coated NFC conductive thread antenna (49.5 mm × 49.5 mm) with a Q value of 8.85, and a stainless steel-coated conductive thread antenna (49.5 mm × 49.5 mm) with a Q value of 4.75 [R1]. Lin *et al.* reported a silver-coated conductive thread NFC antenna (60 mm diameter) with a Q value of 6.5 [R2]. Our designed silver-coated conductive thread antenna (40 mm diameter) has a quality factor of 5.3, aligning with these figures for comparable dimensions. In Fig. 4b-f, we intend to highlight the higher quality factor and spectral stability of our coaxially-shielded antenna in comparison to typical counterparts used in wearable technologies.

In the original manuscript, we supplemented the comparison between the coaxially-shielded antenna and a commercial flexible NFC antenna with a similar coverage (Supplementary Fig. 16a, b). We have further enriched this section by measuring the reflection coefficient of the commercial NFC antenna and comparing the results with the conductive thread antenna and coaxially-shielded antenna (Supplementary Fig. 16d-f). The adopted commercial antenna (FXR. 4040. A, 40 mm × 40 mm, Taoglas) is more susceptible to extraneous loading when compared to the coaxially-shielded antenna. Despite its higher unloaded quality factor (59.8 as specified in the datasheet, 54.75 as measured by the impedance analyzer) compared to the coaxially-shielded antenna (33 as measured), the coaxially-shielded antenna presents better quality factor preservation under loadings and is more spectrally stable than the commercial antenna.

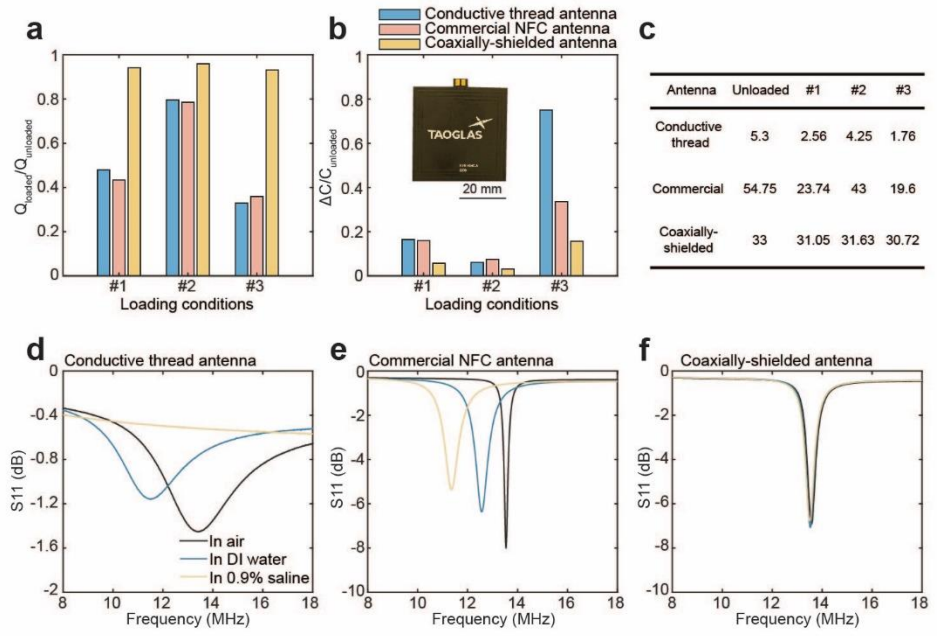

Supplementary Figure 16. Comparison of the coaxially-shielded antenna, conductive thread antenna and commercial flexible NFC antenna. **a** Measured quality factor preservation ($Q_{Loaded}/Q_{Unloaded}$) for the three antennas when affixed to skin (#1), wetted by sweat (#2) and submerged in water (#3). The conductive thread antenna is comparable to the commercial antenna, but both outperformed by the coaxially-shielded antenna. **b** Measured self-capacitance variations $\Delta C/C_{Unloaded}$ for the three antennas. The coaxially-shielded antenna outperforms both the conductive thread antenna and the commercial antenna. Inset: Adopted commercial flexible dual-layered NFC antenna (FXR. 4040. A, 40 mm × 40 mm, Taoglas). **c** Quality factor values as measured in **a**. **d-f** Measured reflection coefficients for the conductive thread antenna (**d**), the commercial NFC antenna (**e**), and the coaxially-shielded antenna (**f**).

[R1] Jiang, Y., et al. e‐Textile embroidered wearable near‐field communication RFID antennas. *IET Microw, Antennas Propag.* **13**, 99-104 (2019).

[R2] Lin, R., et al. Digitally-embroidered liquid metal electronic textiles for wearable wireless systems. *Nat. Commun.* **13**, 2190 (2022).

7. A demonstration of the sensor network in swimming is crucial to support the claim of high robustness.

We thank the reviewer for the suggestion. In response, we conducted additional experiment as presented in Supplementary Figure 18. A metamaterial BAN was constructed on the back of the athletic pants. The reading device (smartphone) was sealed in a waterproof pouch and placed on the left calf to wirelessly power the sensing node on the right knee. Several battery-free energy-harvesting LED nodes were placed along the BAN, indicating robust underwater power transfer. The entire system, including the reader, nodes and the metamaterial, was immersed in tap water. Bending was then performed at the right knee to simulate a swimming scenario, with the resistance values of the strain sensor indicating the degree of knee flexion. The results demonstrate that the metamaterial remains robust and reliable in an underwater environment. We have added a statement to address these results:

"Additionally, to further demonstrate the robustness of the BAN, we construct a metamaterial-enabled BAN on athletic pants for real-time data readout underwater, simulating a swimming scenario. The metamaterial remains functional due to its improved spectral stability, enabling uninterrupted real-time data readout using a smartphone while powering several LED energy-harvesting nodes (Supplementary Fig. 18)." **(Page 21)**

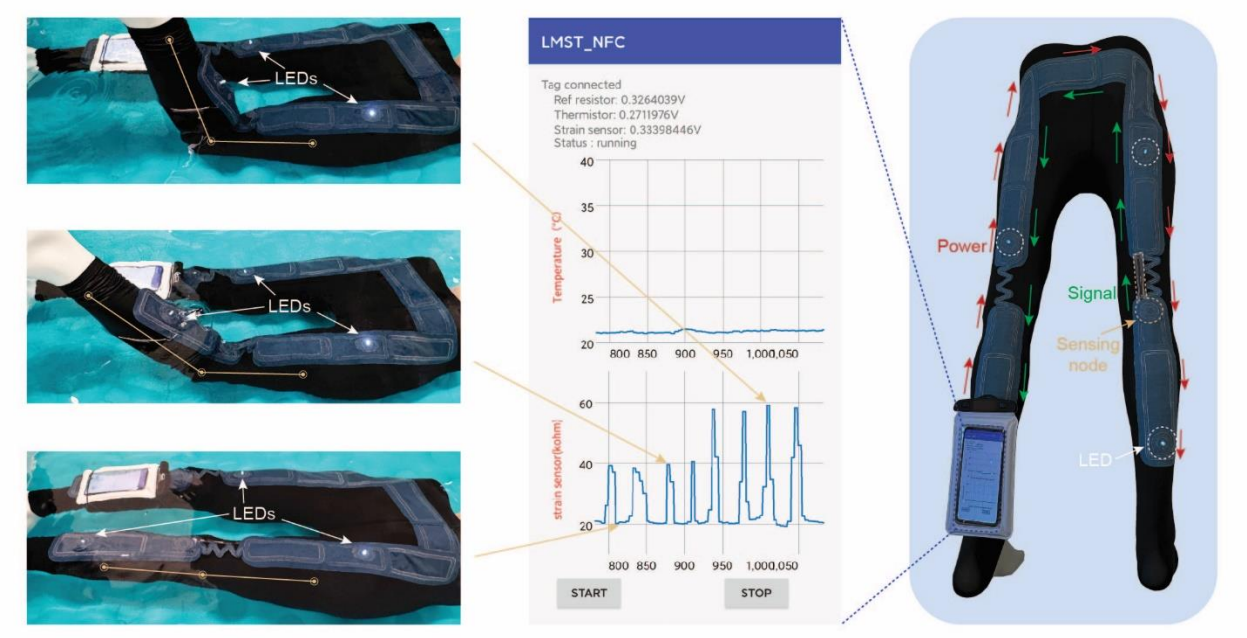

Supplementary Figure 18. Real-time data readout performed underwater. Benefiting from the introduced spectral stability, the metamaterial-enabled BAN promotes reliable underwater real-time data readout. The smartphone, placed in a waterproof pouch, continuously retrieve data from the sensing node, with the strain sensor's resistance indicating the degree of knee flexion, while powering several distant battery-free energy-harvesting LED nodes placed along the BAN.

Reviewer #3:

This article presents an innovative approach to enhancing the functionality of body area networks (BANs) through the integration of Near-Field Communication (NFC) technology into textile metamaterials. The design and implementation of textile metamaterial patch units to improve the NFC communication range within a BAN is both intriguing and practical, especially for wearable technology applications. The detailed explanation of the metamaterial's structure and its impact on spectral stability and environmental resilience is commendable. However, the scientific contribution of this work appears limited. While the extension of the NFC communication range is noteworthy, similar concepts were demonstrated on BANs before: Nat Commun 13, 2190 (2022); Nat Commun 11, 444 (2020). Here are some technical comments:

1.The paper presents a design of a coaxially-shielded textile metamaterial for near-field communication in BANs. To strengthen the scientific contribution of this paper, it would be beneficial to include comparative analyses with existing BAN technologies, specifically assessing power consumption, data transmission efficiency, and user ergonomics. Additionally, exploring how this NFC-enabled BAN design could be optimized for different use cases, including medical monitoring and athletic performance, could provide a more comprehensive understanding of its applicability and limitations.

We thank the reviewer for suggesting these potential investigations to enrich our research. We have provided a comprehensive comparison of the coaxially-shielded metamaterial-based BAN with some recent textile-based BAN technologies, as detailed in Supplementary Table 1, with some comments below.

Supplementary Table 1. Comparison of recent textile BAN technologies.

Reference	This work	S1	S2	S3	S4	S5
Wireless communication technology	NFC (13.56 MHz)	NFC (13.56 MHz)	NFC (13.56 MHz)	NFC (13.56 MHz)	Bluetooth (2.4 GHz)	Modified RFID & Bluetooth
Signal transmission	MI surface wave	Conductive relay	Conductive relay	MI surface wave	Surface plasmon	Radiative (over the air)
Sampling rate	Up to 25 Hz (26.48 kbps data rate)	Up to 8 Hz (26.48 kbps data rate)	Up to 12 Hz (26.48 kbps data rate)	Up to 32 Hz (26.48 kbps data rate)	Up to 1 Mbps data rate	Up to 4 Mbps data rate
Composition of signal transmission relay	Off-the-shelf coaxial cable	Encapsulated conductive thread	Liquid metal tube	Copper/aluminum foil	Off-the-shelf conductive fabric	No relay (over the air)
Clothes integration	Washable hemming tape	Irreversible Embroidery	Irreversible Embroidery	Heat-transferred vinyl	Fabric adhesive	Double-sided tape
Reader/sensor placement	Up to user	Pre-determined terminal/hub	Pre-determined terminal/hub	Up to user	Up to user	Up to user (each sensor require separate initiator)

Measures for improved spectral stability	Coaxially-shielded internal structure	NO (spiral inductive pattern)	NO (spiral inductive pattern)	Ground layer (spiral inductive pattern)	Ground layer (harnessed the sensitivity for sensing capability)	NO (spiral inductive pattern)
Sensitivity to water immersion	Insensitive (coaxially-shielded)	Sensitive	Sensitive	Sensitive	Sensitive	Sensitive
Washability	Multiple machine-washing	Unclear	Multiple machine-washing	20-min hand-washing	Unclear	Can be removed during washing

Power consumption. In existing BAN technologies, a powered reader is essential for collecting the sensor data, regardless of the BAN's configuration. What distinguish these technologies is their signal transmission methods that distribute power to individual sensors, which include surface MI inductive wave, conductive relay, surface plasmon, or over-the-air radiative transmission. It is important to emphasize that the novelty and focus of our work primarily lies in the development of the coaxially-shielded metamaterial, designed to mitigate power loss in a lossy environment. The metamaterial acts as a passive transmission relay with a resonance frequency matched to 13.56 MHz, making the metamaterial compatible with and beneficial to all existing NFC reader/transponder setups.

The power consumption is highly dependent on the adopted devices; therefore, it is unrealistic to source specific values from existing literatures, which often utilize smartphones of different brands or readers equipped with various ICs for advanced development functionalities. However, it is generally observed that near-field techniques like NFC typically consume less power compared to far-field techniques such as Bluetooth, which usually require a separate power source at the sensor end as well. Specifically, we used a USB power monitor to directly measure the adopted reader's circuit board power consumption (Supplementary Fig. 19a). The power consumption of the reader is consistent once plugged in, fluctuating between 0.556 and 0.584 W, presenting no noticeable correlation with the number of sensing nodes being powered or whether the metamaterial BAN was employed. Additionally, we tested another NFC reader from a different vendor (ST25R3911B-DISCO, St Microelectronics), also finding consistent power consumption fluctuating between 1.008 and 1.033 W under these conditions. This result proves that the metamaterial achieves the enhanced communication range without additional power consumption. We have addressed this point in the manuscript along with question 4.

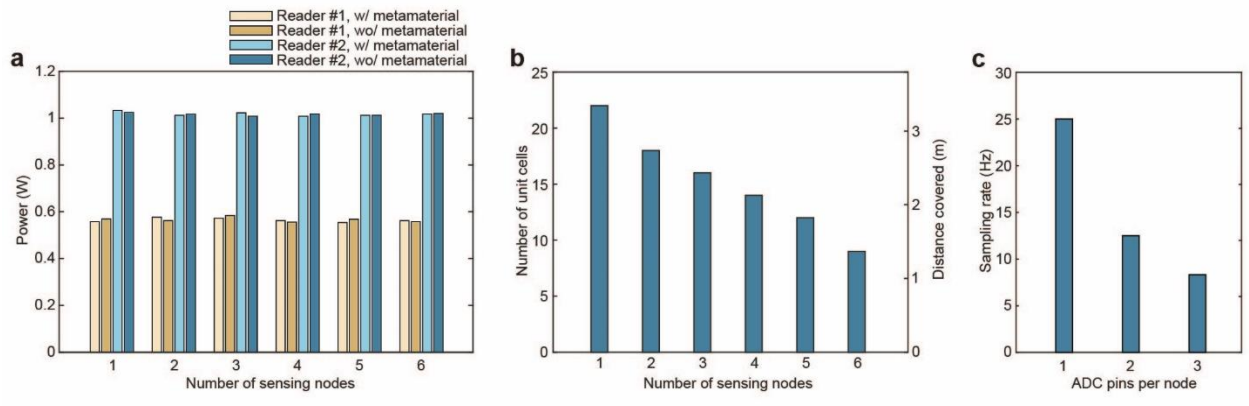

Supplementary Figure 19. Scaling of the BAN's performance with the number of nodes and sensors per node. a Measured power consumption of the adopted reader's circuit board (#1) and an alternative reader's circuit board (ST25R3911B-DISCO, St Microelectronics, #2) while powering different numbers of sensing nodes, with or without the metamaterial. This indicates that the metamaterial enhances the communication range without additional power consumption. **b** The maximum possible number of unit cells in an inline metamaterial array and the distance covered, supporting the associated number of equally spaced sensing nodes. **c** The highest sampling rate for different numbers of ADC pins being sampled in each sensing node.

Data transmission efficiency. In our demonstration, the adopted data sampling rate for each transponder is set to 5 Hz, which is sufficient for the proof-of-concept demonstration of temperature and gait monitoring. Data transmission efficiency hinges on the NFC communication protocol and the specific transponder used. The NFC transponder (RF430frl152h) featured in this study supports three ADC input pins, accommodating up to three analog sensors. In our configuration, two sensors are utilized alongside a reference resistor (100 kΩ) connected to an ADC input for thermistor calibration (Fig. 4a). According to the transponder's datasheet, sampling each analog sensor requires a minimum of 40 ms, setting the maximum sampling rate at 8.33 Hz (120 ms total sampling time) when all three ADC pins are used. The sampling rate decreases inversely with the number of analog sensors connected at each node (Supplementary Fig. 19c). We acknowledge that this level of sampling rate is not adequate for certain important applications, such as electrocardiogram monitoring. However, the data transmission efficiency aligns with other NFC-based BANs, constrained by the inherent limitations of NFC technology, initially designed for simple information exchanges over short distances.

User ergonomics. The construction of the metamaterial involves modifying commercially-available coaxial cable and computer-aided embroidery process. This approach is more convenient than constructing conductor patterns from raw materials. Integration of the BAN into clothing is facilitated using heat-fusible washable hemming tape. The fabric substrate of the metamaterial allows for flexible attachment options, including conventional sewing and hook-and-loop fasteners, making it adaptable to various types of apparel. Importantly, the customizable arrangement of the metamaterial pattern enables the user to strategically place their reader and sensing nodes on their desired positions, such as clothing pockets or directly mounted on the body, a feature not accessible for designs involving permanent embroidery patterns and predetermined terminal positions.

Optimization with different use cases. As further explained in question 4. The metamaterial is completely passive and is designed to interact seamlessly with any NFC-enabled devices without modifications. Subsequently, the optimization of the metamaterial for specific use cases depends solely on the arrangement of the metamaterial to ensure coverage extends to the appropriate sensor/reader locations for each case. Here we provide a few practical considerations for reference (Supplementary Fig. 20).

- **Glucose monitoring.** The metamaterial BAN can enable continuous blood glucose readings from commercial NFC-enabled glucose sensors (e.g., Freestyle Libre 3 by Abbott), recommended to be mounted on the upper arm. Real-time readings can be directly accessed on an NFC-enabled smartwatch or smartphone (Supplementary Fig. 20a).
- **Gait monitoring.** The metamaterial can be integrated with strain sensors mounted on the knee to monitor knee flexion, and with a gyroscope/accelerometer mounted on the ankle to monitor stride time and stride time variability (STV). These are crucial metrics for diagnosing gait abnormalities. For athletes, particularly runners, maintaining consistent knee flexion and minimal STV is desirable for enhancing performance and reducing injury risk (Supplementary Fig. 20b).

- **Spinal posture analysis.** Integrating strain sensors for spinal posture monitoring provides a non-invasive method to assess spinal health. This approach is beneficial for managing musculoskeletal disorders and aiding physical therapy. The flexibility of the BAN allows sensors to be placed along any segment of the spine, adapting to individual needs and therapy requirements (Supplementary Fig. 20c).

These potential application scenarios have been addressed in the manuscript:

"The metamaterial patch unit is constructed individually and then transferred onto clothing using a heat-fusible tape, avoiding an irreversible embroidery process while providing users with maximum flexibility in sensor placement, as shown in the potential metamaterial patterns involving various sensing functionalities (Supplementary Fig. 20)." **(Page 22)**

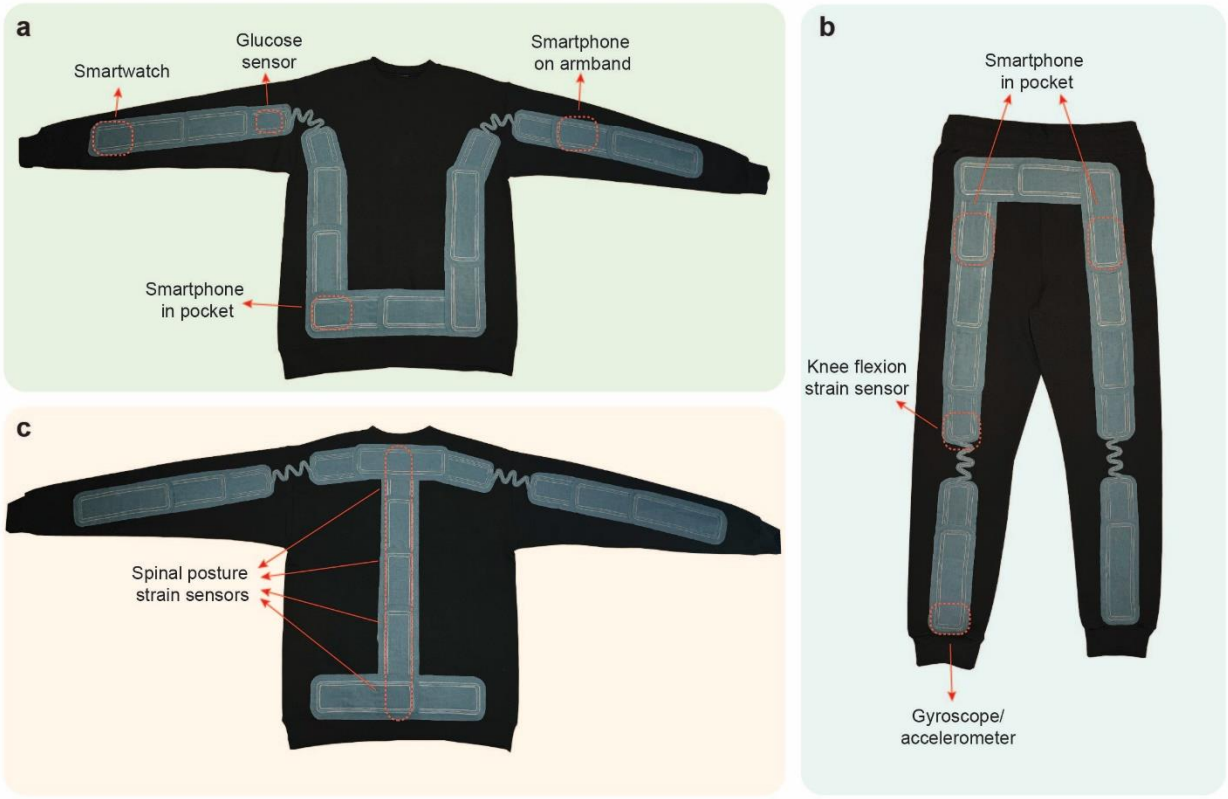

Supplementary Figure 20. Alternative metamaterial patterns with their potential sensing capabilities. **a** The metamaterial enables continuous blood glucose readings on smartphone or smartwatch from commercial NFC-enabled glucose sensors (e.g., Freestyle Libre 3 by Abbott, recommended to be mounted on the upper arm). **b** The metamaterial can be integrated with strain sensors mounted on the knee to monitor knee flexion, and with a gyroscope/accelerometer mounted on the ankle to monitor stride time and stride time variability. **c** The metamaterial enables placement of strain sensors for spinal posture analysis on any segment of the spine.

[S1] Lin, R., et al. Wireless battery-free body sensor networks using near-field-enabled clothing. *Nat. Commun.* **11**, 444 (2020).

[S2] Lin, R., et al. Digitally-embroidered liquid metal electronic textiles for wearable wireless systems. *Nat. Commun.* **13**, 2190 (2022).

[S3] Hajiaghajani, A., et al. Textile-integrated metamaterials for near-field multibody area networks. *Nat. Electron.* **4**, 808-817 (2021).

[S4] Tian, X., et al. Wireless body sensor networks based on metamaterial textiles. *Nat. Electron.* **2**, 243-251 (2019).

[S5] Niu, S. et al. A wireless body area sensor network based on stretchable passive tags. *Nat. Electron.* **2**, 361–368 (2019).

2.The demonstration of spectral stability and reduced sensitivity to external conditions, such as water immersion and mechanical deformation, is impressive. However, the paper could provide more quantitative data on the efficiency of energy transfer within the BAN.

We thank the reviewer for suggesting more quantitative analysis of the energy transfer efficiency within the BAN. As suggested by other reviewers, we have supplemented the adopted setups with detailed metrics for Fig. 2e-g, as shown in Supplementary Figure 25. We have conducted additional measurement with the metamaterial being under various mechanical deformation and loading (Supplementary Fig. 11). The energy transfer efficiency (η) within the BAN is evaluated with increasing number of bends, extents of bending, winding angles, and the salt concentration during water immersion. The setup adopted here is the same as that in Fig. 2e-h, a 12-unit inline metamaterial array. The efficiency η was directly measured by the vector network analyzer and normalized to the case when no deformation or loading was applied to the metamaterial (η_{ref}).

When adopting different number of bends N, or different winding angle θ (maintaining 600 mm pitch), the power transfer within the BAN remains very stable, fluctuating around the reference value with deviations of less than 15% (Supplementary Fig. 11a, c). This indicates the metamaterial's resilience against frequency detuning when conformed to anatomic regions with significant curvature. However, with smaller bending diameters (D), the power transfer efficiency significantly decreased due to increased magnetic flux overlap between adjacent unit cells, severely affecting the metamaterial's resonance (Supplementary Fig. 11b). This indicates that placing the metamaterial on joints, where a wide degree of flexion and random bending/creasing of clothing frequently occurs, may result in substantial power loss. This further highlights the importance of adopting the stretchable joint unit, which effectively avoids such extreme bending scenarios. Notably, for the water immersion scenario with salt concentration up to the seawater levels (3.5%), the power transfer efficiency is maintained above 50% compared to the unloaded case, highlighting the robustness of the coaxially-shielded metamaterial against dielectric and conductive losses from the surrounding media (Supplementary Fig. 11d). A statement has been added in the manuscript:

"Further measurements show that the presented bending and winding scenarios result in a stable power transfer within the metamaterial. Notably, even when immersed in 3.5% saline, the power transfer efficiency maintains above 50% compared to scenarios with no deformation or loading (Supplementary Fig. 11)." **(Page 13)**

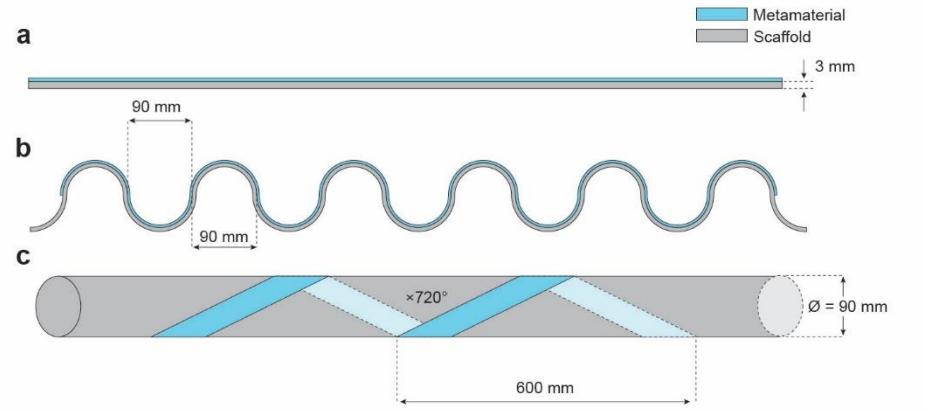

Supplementary Figure 25. **Experimental setup adopted in Figure 2e-g. a** In Fig. 2e, the metamaterial was placed on an acrylic board. **b** In Fig. 2f, the metamaterial was placed on a 3D-printed serpentine PLA scaffold. **c** In Fig. 2g, the metamaterial was wound around an acrylic pipe.

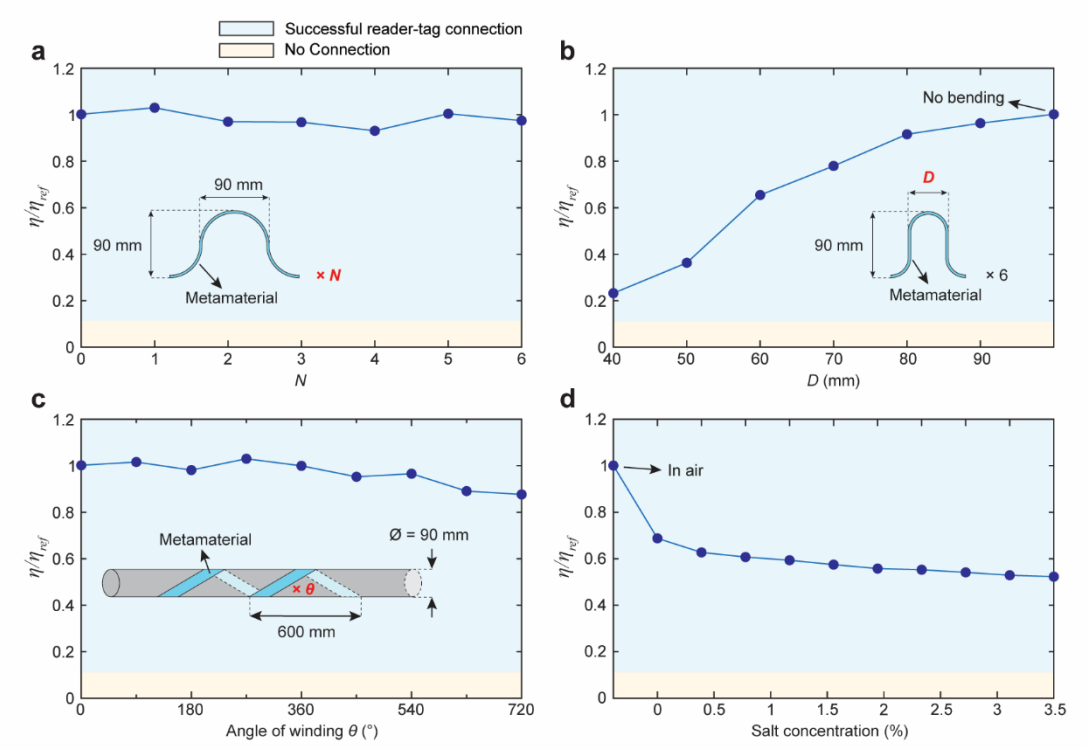

Supplementary Figure. 11. **Variation in the power transfer efficiency within a 12-unit inline metamaterial. a-d** Measured power transfer efficiency (η) within the metamaterial at 13.56 MHz, influenced by the number of bends N (**a**), diameter of each bend D (**b**)**,** winding angle θ (**c**), and the salt concentration when immersed in saline (**d**). The efficiency is normalized to the reference condition with no deformation or loading (η_{ref}). The threshold for successful reader-tag connection is assessed by vertically lifting the sensing node (placed at the metamaterial's end) to the highest readable position by the reader placed at the opposite end. VNA near-field probes are then placed at the positions of the reader and the sensing node.

3.The work emphasizes the scalability and user-customizability of the metamaterial BAN. It would be valuable to discuss the limitations regarding the maximum number of sensor nodes that can be supported and how the network's performance scales with the number of nodes and the distance covered.

We thank the reviewer for suggesting the discussion on the maximum sensing capabilities of the BAN. In radio frequency identification systems, when multiple tags/transponders attempt to transmit signals simultaneously, the signals cannot be distinguished without an anti-collision protocol embedded in the communication protocol [R1]. Specifically, the NFC signal transmission in this work is specified by the ISO 15693 Standard, implemented at both the reader's and the tag's ends. This Standard incorporates the Frame Slotted Aloha (FSA) protocol to solve the potential collision issues, thereby aligning with the industrial standards for multi-transponder communication [R2]. Particularly, this FSA protocol prompts all tags to randomly select one of the available time slots to transmit their unique identifiers. In instances where multiple tags respond in the same time slot, resulting in a collision, the reader instructs the colliding tags to retransmit in different slots, and this process is repeated until all tags are successfully identified. The adopted NFC reader (DLP7970-ABP, TI) is integrated with the TRF7970A NFC transceiver IC, which accommodates a total of 16 such time slots [R2]. Consequently, the maximum number of tags supported is 16 in this implementation. This has been indicated in the Methods Section:

"Communication between the reader and the tags followed the ISO 15693 standard, incorporating the Frame Slotted Aloha anti-collision protocol. This protocol iteratively instructs individual tag to transmit signal in a unique, unoccupied time slot. The maximum number of tags that can be supported, which is defined by the available time slots in the reader, is 16 in this implementation." **(Page 26)**

Regarding the network's performance in relation to the number of nodes and distance covered, we adopted an inline metamaterial array with an increasing number of unit cells to test the scalability. When only one node is used, the metamaterial can extend the communication range up to 22 unit cells (≈3.35 m). When multiple sensing nodes are integrated, the distribution of power into additional sensing nodes is evidenced by a decrease of the longest possible distance covered (Supplementary Fig. 19b), which is measured with the associated number of nodes spaced roughly equally along the inline metamaterial. This has been addressed in the Methods Section:

"The three tags were strategically placed under the armpit, on the elbow, and on the waist, with wireless communication distances of 0.4 m, 1 m and 0.9 m along the metamaterial relay separately. The effect of integrating multiple tags is evidenced by a decrease of the longest possible distance covered due to power distribution to individual tag (Supplementary Fig. 19b)." **(Page 26)**

[R1] Klair, D. K., Chin, K.-W. & Raad, R. A survey and tutorial of RFID anti-collision protocols. *IEEE Commun. Surv. Tutor.* **12**, 400–421 (2010).

[R2] Corches, C., Daraban, M. & Miclea, L. Availability of an RFID object-identification system in IoT environments. *Sensors* **21**, 6220 (2021).

4. The integration of NFC-enabled sensing nodes with commercial NFC readers and smartphones is a practical aspect of this study. However, more details on the compatibility, required modifications, or limitations when integrating with various brands or types of smart devices could provide a clearer view of its applicability in real-world scenarios.

We thank the reviewer for suggesting additional clarifications on the practical aspect of our work. As mentioned, the NFC reader-to-tag communication in this work is specified by the ISO 15693 Standard. This

communication protocol is implemented in both the adopted NFC transponder (RF430frl152h, TI) and the commercial NFC reader (DLP-7970ABP, TI). Our near-field metamaterial does not and is not capable of modifying this protocol; instead, it only serves as a passive transmission relay to extend the communication range of the NFC reader from a few centimeters to the scale of the human body. The metamaterial is designed to interact uniformly with any signal within the NFC band. As such, the metamaterial is compatible with all NFC-enabled readers and tags, as long as their working frequency is centered at 13.56 MHz.

It is our understanding that, as of drafting this response, most mainstream smartphones are equipped with the NFC technology, and these smartphones typically support various NFC communication protocols, including ISO 15693, ISO 14443, and more. In fact, the commonly-adopted mobile payment systems rely on the NFC technology, which is integrated into the most popular Android and iOS operating systems. The smartphone adopted for data readout in our study is a Xiaomi phone that adopts the Android operating system, NFC capabilities were integrated into the phone's chip by the manufacture; we have conducted no modifications to the operating system or the hardware. In terms of commercial NFC readers, they are primarily developed for development purposes, thereby usually support a broad range of NFC communication protocols. Therefore, no modifications are required on the reader's or tag's side when integrating with different brands or types of smart devices. We have added a discussion on compatibility with NFC devices in the discussion:

"Specifically, the sensor readout adopted herein follows the ISO 15693 Standard, implemented at both the reader's end and the sensing nodes' end. The use of the metamaterial does not alter the communication protocol or the power consumption of the reader (Supplementary Fig. 19a); instead, it acts as a passive signal transmission relay matched to the NFC working frequency, allowing it to extend the power distribution to distant sensing nodes that are beyond the reach of conventional NFC technology. The metamaterial is engineered to uniformly interact with any signal within the NFC band, ensuring universal compatibility with all NFC-enabled devices without requiring modifications." **(Page 22)**

5. While the paper touches on the durability of the metamaterial in harsh conditions, long-term wear and maintenance aspects, such as the ease of repairing or replacing parts of the BAN, are not thoroughly discussed. Insights into these practical aspects would enhance the understanding of the technology's viability for everyday use.

We thank the reviewer for suggesting more discussion into the long-term wear and maintenance aspects.

It is true that RF components in wearable technologies often face breakdowns during long-term wear. In our study, the metamaterial unit cells are individually constructed and then assembled on existing clothing. The RF communication between adjacent unit cells is achieved through wireless inductive coupling. Since there are no physical connections between the coaxial cable in adjacent unit cells, this configuration naturally facilitates easy of replacement. We used heat-fusible, washable hemming tape for adhesion, which remains effective after washing. We have tested that individual metamaterial patch units can be removed by force without damaging the clothing or the metamaterial. Repairing the internal coaxial structure of the metamaterial, on the other hand, is challenging. However, given that coaxial cables are often mass-produced and cost-effective, we recommend replacing damaged parts rather than repairing them. We have added a discussion on these practical aspects in the manuscript:

"The metamaterial patch unit is constructed individually and then transferred onto clothing using a heat-fusible tape, avoiding an irreversible embroidery process while providing users with maximum flexibility

in sensor placement, as shown in the potential metamaterial patterns involving various sensing functionalities (Supplementary Fig. 20). Meanwhile, this strategy naturally simplifies the replacement of broken parts during long-term wear, as the cable-based resonators in adjacent unit cells are not physically interconnected. Although repairing the intricate coaxial structure within the cable remains challenging, replacing the unit cells is cost-effective due to the mass production and widespread availability of coaxial cables." **(Page 23)**

REVIEWERS' COMMENTS

Reviewer #1 (Remarks to the Author):

The authors have fully addressed my previous comments.

Reviewer #2 (Remarks to the Author):

1. Comment 3.

“The selected dimension of the micro coaxial cable (diameter 0.99mm) balances ease of fabrication and flexibility, resulting in a lightweight, nearly imperceptible, and comfortable BAN for the user.”

“Regarding the trade-off between cable size, flexibility, and user comfort, the authors believe this relationship is straightforward: thinner wire with the same composition is naturally more flexible and less noticeable when worn.”

Sure, a thinner wire with the same composition is naturally more flexible and less noticeable when worn. However, this does not support the claim that the micro coaxial cable is nearly imperceptible and comfortable. I don’t believe that a coaxial cable with 1mm diameter is nearly imperceptible and comfortable .To support this claim, the coaxial cable should be compared with the materials typically used in clothing.

2. Comment 4.

“In sharp contrast to previous efforts to develop NFC-enabled wearable BANs based on spiral-based inductive patterns24-26, the metamaterial proposed herein demonstrate remarkable spectral stability and insensitivity against extraneous loadings (Supplementary Fig. 1).”

However, Supplementary Fig.1 didn’t involve References [Hajiaghajani, A., Nature Electronics, 4(11), 808-817, 2021] and [Hajiaghajani, A., Nature Communications, 14(1), 7522, 2023], which have demonstrated spectral robustness against skin and water.

Reviewer #3 (Remarks to the Author):

The authors well addressed all my concerns that I would like to recommend it to be accepted by Nature Communications.

We thank the reviewer for their follow-up comments on the wording and references in our manuscript. Please find below a point-by-point response where the original comment from the reviewer is marked in green. The specific changes made to the manuscript are highlighted in blue.

1. Comment 3.

"The selected dimension of the micro coaxial cable (diameter 0.99mm) balances ease of fabrication and flexibility, resulting in a lightweight, nearly imperceptible, and comfortable BAN for the user."

"Regarding the trade-off between cable size, flexibility, and user comfort, the authors believe this relationship is straightforward: thinner wire with the same composition is naturally more flexible and less noticeable when worn."

Sure, a thinner wire with the same composition is naturally more flexible and less noticeable when worn. However, this does not support the claim that the micro coaxial cable is nearly imperceptible and comfortable. I don't believe that a coaxial cable with 1mm diameter is nearly imperceptible and comfortable. To support this claim, the coaxial cable should be compared with the materials typically used in clothing.

We thank the reviewer for addressing concerns regarding expressions such as "nearly imperceptible" and "comfortable". We agree that these statements are subjective and inappropriate without scientific validations.

In response, we have revised the previous statement, replacing these subjective terms with objective descriptions:

"*The selected dimension of the micro coaxial cable (diameter 0.99mm) balances ease of fabrication and flexibility, resulting in a lightweight and conformable BAN.*" **Page 23**

We have carefully reviewed the manuscript to ensure it is free of such subjective descriptions.

2. Comment 4.

"In sharp contrast to previous efforts to develop NFC-enabled wearable BANs based on spiral-based inductive patterns24-26, the metamaterial proposed herein demonstrate remarkable spectral stability and insensitivity against extraneous loadings (Supplementary Fig. 1)."

However, Supplementary Fig.1 didn't involve References [Hajiaghajani, A., Nature Electronics, 4(11), 808-817, 2021] and [Hajiaghajani, A., Nature Communications, 14(1), 7522, 2023], which have demonstrated spectral robustness against skin and water.

We thank the reviewer for addressing this issue. We agree with the reviewer that including "*Reference 25: Nature Electronics, 4(11), 808-817, 2021*" in the addressed statement is inappropriate. In Reference 25, the authors introduced a ground layer with uniformly patterned slots, positioned in close proximity to the spiral-based inductive patterns, which is then integrated between heat-transfer vinyl layers to improve the BAN's spectral stability. We have removed Reference 25 in this statement. In Reference 25, the metamaterial only demonstrates moderate spectral stability on the human body's side, and remains sensitive to salted water,

even when only 90 cm^2 of the metamaterial was wetted, as evidenced in Supplementary Figure 14 in Reference 25 [R1].

In the previous version of our manuscript, efforts in Reference 25 have been addressed prior to the outlined statement:

"These concerns were addressed in a textile-integrated resonating loop array (metamaterial), where the NFC signal may be transmitted through inductive coupling along the resonator array in the form of a magneto-inductive wave, enabling connectivity with multiple sensors placed at arbitrary positions along the BAN[25]. This approach involves a resonator design cut from metal foil and a slotted ground metal foil layer, integrated onto pre-existing clothing. While the design demonstrates moderate spectral stability on just one side, it remains sensitive to more extreme loading, such as water. In addition, the mechanical durability of the slotted metal foil design remains questioned during daily wear." **Page 3**

Regarding efforts in "*Nature Communications, 14(1), 7522, 2023*", the authors reported an epidermal solution with spectral stability enabled by integrating lumped surface mount capacitors and PDMS sheets to encapsulate the silver ink-based conductive patterns. This approach increases the overall construction complexity and internal fragility. We are unable to replicate such a configuration due to the lack of similar fabrication techniques and machinery. However, our manuscript primarily focuses on demonstrating a novel metamaterial with a coaxially-shielded internal structure, a simple and straightforward strategy suitable for constructing RF components in various near-field application scenarios. The coaxially-shielded structure can achieve spectral stability against water even without additional lumped capacitors or insulating sheets. This key difference has been previously addressed in the discussion section:

"Moreover, our metamaterial design intentionally introduces a substantial structural capacitance to bind the electric field within the layered internal structure, imparted by industrially certified coaxial cable. This simple, straightforward design minimizes undesired interference with the surrounding environment with minimal effort, while eliminating lumped elements and fragile internal structures proposed elsewhere[25,49]." **Page 23**

[R1] Hajiaghajani, A., et al. Textile-integrated metamaterials for near-field multibody area networks. Nat. Electron. 4, 808-817 (2021). [Supplementary information]